A vinculin-binding domain from the talin rod unfolds to form a complex with the vinculin head.

Ian Fillingham, Alexandre R. Gingras, Evangelos Papagrigoriou[§], Bipin Patel, Jonas Emsley[§], David R. Critchley, Gordon C.K. Roberts and Igor L. Barsukov[¶]

Department of Biochemistry

University of Leicester

University Road

Leicester, LE1 7RH

United Kingdom

[§] Present address: School of Pharmacy, University of Nottingham, University Park, Nottingham NG7 2RD, UK

[¶] Corresponding author: Phone +44 (0)116 252 3055; Fax +44 (0)116 223 1503; Email igb2@le.ac.uk

Abstract

The cytoskeletal protein talin plays a key role in activating integrins and in coupling them to the actin cytoskeleton. Its N-terminal globular head, which binds β-integrins, is linked to an extended rod having a C-terminal actin-binding site and several vinculin-binding sites (VBSs). The NMR structure of residues 755-889 of the rod (containing a VBS) is shown to be an amphipathic 4-helix bundle with a left-handed topology. A talin peptide corresponding to the VBS binds the vinculin head; the X-ray crystallographic structure of this complex shows that the residues which interact with vinculin are buried in the hydrophobic core of the talin fragment. NMR shows that the interaction involves a major structural change in the talin fragment, including unfolding of one of its helices, making the VBS accessible to vinculin. Interestingly, the talin 755-889 fragment binds more than one vinculin head molecule, suggesting that the talin rod may contain additional as yet unrecognised VBSs.

The integrin family of transmembrane αβ heterodimers are important in both cell-cell and cell extracellular matrix interactions. In most, though not all, cases they are coupled to the actin cytoskeleton via proteins such as talin, α-actinin, filamin and tensin (Liu *et al.,* 2000), a link which is important to actomyosin-driven cell migration and the signalling pathways that regulate cell proliferation and apoptosis. Microinjection of talin antibodies (Nuckolls *et al.,* 1992; Bolton *et al.,* 1997) or talin polypeptides (Hemmings *et al.,* 1996), and down-regulation of talin using antisense RNA technology (Albiges-Rizo *et al.,* 1995) or gene knockout (Priddle *et al.,* 1998; Monkley *et al.,* 2000; Brown *et al.,* 2002; Cram *et al.,* 2003) all demonstrate that talin plays a key role in integrin-mediated adhesion and developmental events. Moreover, talin has recently been shown to activate integrins (Tadokoro *et al.,* 2003) by dissociating the interaction between the α/β-cytoplasmic domains (Kim *et al.,* 2003). The biochemical and structural properties of talin are also consistent with such a role. It is an elongated (2541 residues; 60 nm) flexible anti-parallel dimer, with a small globular head connected to an extended rod (Winkler *et al.,* 1997). The talin head contains a FERM domain with binding sites for several β-integrin cytodomains (Calderwood, 2004) as well as for type 1γ PI4'5'-kinase (Di Paolo *et al.,* 2002; Ling *et al.,* 2002), which is involved in focal adhesion assembly, and the tyrosine kinase FAK (Chen *et al.,* 2002), which is important in focal adhesion turnover and cell migration. The structure of part of the talin FERM domain identifies a PTB-like domain that binds both to the membrane proximal NPxY motif in the β3-integrin cytodomain (Garcia-Alvarez *et al.,* 2003) and to PI4'5'-kinase (Barsukov *et al.,* 2003). The talin rod contains a second lower affinity integrin-binding site (Xing *et al.,* 2001; Tremuth *et al.,* 2004), a highly conserved C-terminal actin-binding site (McCann and Craig, 1997), and at least three vinculin binding sites (VBSs; Hemmings *et al.,* 1996; Bass *et al.,* 1999); vinculin in turn has multiple binding partners including F-actin (Jockusch and Rudiger, 1996). Current data suggest that integrin-mediated adhesion triggers the translocation of a complex of talin with PI4'5'-kinase to the membrane, resulting in localized production of PIP2 (Ling *et al.,* 2002) which activates the integrin-binding site(s) in talin (Martel *et al.,* 2001). Talin then binds, activates and couples integrins to F-actin, and studies using talin1(-/-) fibroblasts show that talin is indeed required to support the initial weak interaction between integrins and actomyosin (Jiang *et al.,* 2003) and the assembly of focal complexes (Giannone *et al.,* 2003). PIP2 also activates vinculin (Gilmore and Burridge, 1996) which, although not required for focal adhesion assembly *per se*, is important in the regulation of cell migration (Xu *et al.,* 1998).

The structures of vinculin subdomains have been determined (Bakolitsa *et al.,* 1999; Izard *et al.,* 2004), including complexes of the vinculin head (residues 1-258) bound to synthetic talin peptides containing minimal vinculin binding sites (Izard *et al.,* 2004; Papagrigoriou *et al.,* 2004; Izard and Vonrhein, 2004), corresponding to VBS1 and VBS3 identified earlier (Hemmings *et al.*, 1996; Bass

et al., 1999). Recently, we described the structure of the N-terminal part of the talin rod (residues 482-789; Papagrigoriou *et al.,* 2004), a region which contains the vinculin-binding site VBS1. The residues involved in vinculin binding align on the hydrophobic face of an amphipathic helix that is normally buried within the hydrophobic core of a five helix bundle. We now report the solution structure of an adjacent region of the talin rod (residues 755-889) that contains another vinculin binding site, VBS2, together with studies of its interaction with the vinculin head by crystallography and NMR. We show that this region is also a helical bundle, and combine the new structural information with our earlier work to propose a model for the structure of the N-terminal 400 residues of the talin rod. We show that the interaction of talin VBS2 with vinculin is similar to that reported for VBS3 (Izard *et al.,* 2004) and, importantly, that this interaction requires a major structural change in talin 755-889, including complete unfolding of one of its four helices.

Results

Structure of the talin 755-889 fragment

Talin 755-889 in solution gives a well-resolved NMR spectrum, with linewidths indicating that it is a monomer. The resonances have been assigned by conventional triple-resonance experiments using [^{13}C,^{15}N]-labelled protein, and the solution structure has been determined using 3018 distance constraints from NOEs and 176 dihedral angle constraints from scalar couplings. The N-terminal (755-766) and the C-terminal (884-889) residues are unstructured and flexible, as indicated by the relatively weak intraresidue and sequential NOEs and narrow lines observed for these regions. The core of the fragment, residues 767 to 883, forms an up-down-up-down four-helix bundle (Figure 1a,b) with the helices connected in a left-handed topology. All four helices in the bundle are α-helices, well characterised by an extensive set of HN_i/H^{α}_{i-3}, HN_i/H^{α}_{i-4} and $H^{\alpha}_i/H^{\beta}_{i+3}$ NOEs. The helices are straight and nearly antiparallel, with a small angle between the pairs of helices H1+H2 and H3+H4. Helices H1, H3 and H4 have similar lengths of ~25 residues, while helix H2 is notably shorter (~18 residues). Helices H2 and H3 are connected by a short tight loop, a slightly longer and less structured loop connects helices H3 and H4, but helices H1 and H2 are linked by a much longer unstructured loop of 12 residues.

All four helices of talin 755-889 are amphipathic, with their more hydrophobic surfaces buried in the interior of the bundle, which is made up of two distinct hydrophobic clusters separated by polar uncharged residues (Figure 1b). The larger cluster is positioned at the end of the bundle where the N- and C-termini of the fragment are located; its core is formed by three methionine side-chains (816, 822 and 870) that make extensive contacts with a large number of aliphatic side-chains. Residues 816 and 822 are at opposite ends of the tight turn between helices H2 and H3 and Met 870 is in helix H4. The aromatic ring of Phe813 lies flat on the side of the cluster between the helices H1 and H2, with its other surface exposed to the solvent. At the open end of the bundle, the cluster is partly shielded from solvent by the tight turn between helices H2 and H3 and by the last turn of helix H4. The second hydrophobic cluster is located at the other end of the bundle; the large loop between helices H2 and H3 and the shorter length of helix H2 makes the structure of the bundle open at this end. This second cluster consists mainly of aliphatic side-chains, notably Leu786 from helix H1, Leu836 and Ile840 from H3 and Leu863 from H4. At the open end of the bundle, this cluster is capped by the aromatic ring of Tyr798, the first residue of helix H2. The two clusters are separated by a polar "belt" of threonine residues in the middle of the bundle: Thr775 of helix H1, Thr809 of H2, Thr833 of H3 and Thr867 of H4. These residues make pairwise contacts, with the Thr 775/Thr 809 pair positioned close to the surface of the bundle and the Thr 833/Thr 867 pair more buried.

The surface of the bundle is predominantly made of charged or polar residues. However, there is a relatively large flat hydrophobic patch in the vicinity of Phe813 at the interface between helices H1 and H2, and there is a narrow groove of exposed hydrophobic side-chains at the interface between helices H1 and H4. As discussed below, these hydrophobic regions around helix H1 may be important for domain assembly in the talin rod structure.

Structural comparisons

Using DALI (Holm and Sander, 1997), the overall structure of talin 755-889 was found to be similar to those of several other helical bundle proteins, in particular to invertase inhibitor (PDB 1RJ1, DALI Z-score 12.1, rmsd 2.2Å), to a *de novo* designed protein s-824 (PDB 1p68, DALI Z-score 8.88, rmsd 2.6Å) and to domain 2 (residues 656-789) of the talin rod whose structure we reported recently (Papagrigoriou *et al.,* 2004). The comparison of talin 755-886 and talin 656-789 is shown in Figure 1c (DALI Z-score 11.8, rmsd 2.4Å). All these proteins contain a 4-helix bundle structural motif with a left-handed topology; the left-handed bundle topology is currently much less common than the right-handed in the PDB, these proteins being the only examples. Several proteins with right-handed topology also showed significant similarity to talin 755-889, notably the FAT domain of FAK (PDB 1k40, DALI Z-score 7.3, rmsd 2.4Å) and α-catenin (PDB 1h6g, DALI Z-score 7.2, rmsd 2.6Å). Both left- and right-handed bundles with high Z-scores have similar near-parallel orientation of the helices. All the α-helices of these structures are amphipathic, with the hydrophobic faces of the helices forming the core of the structures and the hydrophilic faces being solvent accessible. The structure of talin 755-889 has additional features resembling those of the FAT domain: a methionine-based cluster at one end of the structure, and a partially buried tyrosine side-chain capping the hydrophobic cluster at the other end.

Notwithstanding these similarities, talin 755-889 has one structural feature that distinguishes it from all the above helical bundles, the large unstructured loop between helices H1 and H2 (Figure 1a,b). The C-terminal end of helix H2 is positioned at the same level as the ends of the other three helices in the bundle, as seen in the helical bundles of the other proteins. However, the N-terminal end of this helix is offset by approximately two helical turns from the end of the bundle, and the H1-H2 loop can be thought of as an unwinding of the N-terminal part of helix H2. The length of this loop (~12 residues) would be sufficient for the helix to be the same length as the others, but the amino acid composition within the loop, in particular the $G_{791}AGPAG_{796}$ sequence (Figure 1d), would make the helical structure unstable. The shorter length of helix H2 makes the structure of the bundle open at the loop end. The H1-H2 loop is large and flexible, while the neighbouring loop connecting helices H3 and H4 is relatively short but unstructured in the region 847-852. The existence of the shorter helix H2, and the predicted decreased stability of the helical bundle may be important for the regulation of the talin-vinculin interaction.

The overall structure of the talin rod

Talin 755-889 overlaps by one helix with the talin 482-789 fragment, which comprises distinct 5- and 4-helix bundles packed together by hydrophobic surface contacts (Papagrigoriou *et al.,* 2004). A simple superposition of the structures based on this common helix (Figure 2a) demonstrates that the surfaces of the helices that are buried inside the 482-789 and 755-889 fragments are distinctly different, so that most of the intra-bundle contacts can be satisfied simultaneously. In addition the 755-889 bundle is positioned on the opposite face of the 656-789 4-helix bundle to that occupied by the N-terminal 482-655 5-helix bundle. However, the simple superposition results in clashes between helices H8 of talin 482-789 and H4 of talin 755-889 and to resolve these some structural rearrangement of the helical bundles from the two fragments must occur.

The feasibility of such a structural rearrangement was assessed by molecular modelling. Intramolecular contacts within individual helical bundles were converted into distance restraints with upper and lower limits adjusted to ensure that the original structures are faithfully reproduced on the basis of these simulated restraints. In addition, backbone dihedral angle restraints for the helical regions were used to maintain the secondary structures. The restraints for the individual domains were then combined and a set of structures were generated, minimising the restraint violations. The resulting models for the fragment 656-889 have ~30 restraints violated by >0.5Å and none violated by >2.0Å, demonstrating the feasibility of a combined structure that preserves the essential features of the experimental structures of the individual fragments.

A representative model of the combined structure is compared with the experimentally determined structures of the individual fragments in Figure 2b,c. The model demonstrates that the clash between the fragments 482-789 and 755-889 in a simple superposition can be relieved by a small readjustment of the orientation of the helices within the individual bundles. This rearrangement leads to a backbone rmsd of 0.7-0.9Å between the experimentally defined helical bundles and the corresponding regions in the combined model, indicating that the structures are closely similar. The resulting model of the region 636-889 is a 7-helix bundle with the helices oriented at small angles relative to each other. The lengths and the relative orientations of the helices make the overall shape of the structure globular and slightly flattened. The contacts between the two 4-helix bundles to form the 7-helix bundle in the combined model are predominantly hydrophobic, and no charged groups are buried. Most of these contacts involve the large hydrophobic surface along helix H9 of the 4-helix bundle 656-789 and the hydrophobic groove between helices H1 and H4 of the 4-helix bundle 755-889, which are solvent exposed in the individual fragments. The surface of the 7-helix bundle is predominantly polar with a relatively small flat hydrophobic patch between helices H1 and H4 of the bundle 755-889.

Since the fragment talin 482-789 comprises distinct 5- and 4-helix bundles (Papagrigoriou *et al.,* 2004), we can add the N-terminal 5-helix bundle comprising residues 482-655 to the 7-helix bundle model for residues 656-889 to obtain a model for the first 400 residues of the talin rod. This model has been obtained by the same kind of minimisation of restraint violations and is shown in Figure 2d.

The binding of a VBS2 peptide to the vinculin head

A peptide corresponding to the vinculin binding site VBS2 (residues 849 to 879; corresponding to helix H4 in talin 755-889) was synthesised; a complex of this peptide with the vinculin head (Vh') crystallised in spacegroup $P2_12_12$. The structure was determined to 2.38Å and refined to an R factor of 0.242 (Supplementary Table 1). One complex is observed in the asymmetric unit with residues 0 to 251 modelled for vinculin and residues 853-876 for the talin peptide. The overall organisation of the Vh'–VBS2 structure is topologically equivalent to that of the Vh'–VBS1 and Vh'–VBS3 complexes reported recently (Izard *et al.,* 2004; Papagrigoriou *et al.,* 2004; Izard and Vonrhein, 2004) and consists of two subdomains. At the N-terminus four helices (α1-α4) from Vh' surround a fifth helix formed by residues 853-876 from the talin VBS2. This domain is connected to the second domain of Vh' through an elongated helix α4. The contacts made between residues in the VBS2 (H4) helix and Vh' are compared to those within the 4-helix bundle of talin 755-889 in Figure 3. The majority are hydrophobic contacts, but with some isolated polar interactions. For example, unlike VBS1 and VBS3, VBS2 has an N-terminal Lys855 sidechain which is able to form a weak salt bridge to Glu59 of Vh'. In all three Vh'–VBS peptide complexes, the carbonyl oxygen of the residue corresponding to VBS2 Ala868 forms a hydrogen bond to the sidechain of Vh' Gln18. The comparison in Figure 3 shows clearly that the hydrophobic face of the amphipathic talin VBS2 (H4) helix is buried within the Vh' complex just as it is within the 4-helix bundle of talin 755-889. It is thus clear that binding of the VBS2 sequence of talin 755-889 to Vh' could only take place if the talin 4-helix bundle structure was disrupted; NMR studies of the formation of this complex demonstrated that this does indeed occur.

The interaction of talin 755-889 with the vinculin head

The formation of the complex between the whole talin 755-889 fragment and the vinculin head (Vh') was monitored by [^{1}H,^{15}N]-HSQC NMR spectra (Figure 4). On addition of unlabelled Vh' to ^{15}N-labelled talin 755-889, the cross-peaks in the spectra corresponding to the free talin decrease in intensity, and disappear when Vh' is in excess. At the same time, a new set of cross-peaks arising from talin 755-889 in complex with Vh' appear in the spectra, and increase in intensity with increasing Vh' concentration. Quantitative titrations showed that complete disappearance of the resonances of free talin 755-889 required addition of an approximately 3-fold molar excess of Vh'.

The stoichiometry of the Vh' – talin 755-889 interaction was assessed independently by native PAGE experiments, using talin 482-636, which we previously showed (Papagrigoriou *et al.,* 2004) to form a 1:1 complex with Vh', for comparison. Titrations were carried out using a fixed amount of each talin fragment (14μM) and increasing amounts of Vh' (3.4 to 55μM). Talin 755-889 migrated as a relatively discrete band (Figure 4d top, lane 1) whereas talin 482-636 (Figure 4d bottom, lane 1), migrated to an apparently anomalous position considering the similarity of the molecular weights and predicted pIs of the two fragments. Previous gel filtration analysis of talin 482-636 showed an anomalously high apparent molecular weight, which was attributed to its extended and partly unfolded structure (Papagrigoriou *et al.,* 2004). Addition of an equimolar amount of Vh' to talin 482-636 resulted in the disappearance of the band corresponding to free talin 482-636 and the appearance of a band corresponding to the complex. Further addition of Vh' led to the appearance of a band corresponding to free Vh' with no increase in the intensity of the complex (Figure 4d bottom, lanes 6-8). This is consistent with the 1:1 stoichiometry of the Vh'–talin 482-636 complex reported earlier (Papagrigoriou *et al.,* 2004). By contrast, in experiments with Vh' and talin 755-889, a band corresponding to the free talin fragment is still present at equimolar concentrations of the two proteins, although there is no free Vh'. The talin band disappears only at [Vh']:[talin 755-889] ratios between 2:1 and 3:1, accompanied by the appearance of a band corresponding to free Vh' (Figure 4d top, lanes 6 and 7). At the same time, the intensity of the band corresponding to the complex increases with increasing Vh' concentration until a 3:1 ratio is reached. A small shift in mobility of the complex is also observed over this concentration range (in contrast to the behaviour of the Vh'–talin 482-636 complex) suggesting an equilibrium between complexes with different stoichiometry. This experiment, together with the NMR titration, suggests that talin 755-889 has the capacity to interact with more than one Vh' molecule simultaneously.

A comparison of the spectra of talin 755-889 in the free form and in complex with Vh' is shown in Figure 4a,b; the characteristics of the [^{1}H,^{15}N]-HSQC spectrum of the complex are clearly very different to those of the corresponding spectrum of the free form. In the spectra of the complex, only ~45 cross-peaks are observed even for [^{2}H,^{15}N]-labelled talin samples, approximately one-third the number observed for the free protein. These cross-peaks can be divided into three groups: a group of relatively sharp intense cross-peaks, a group of substantially broader, but still intense peaks, and finally a number of much weaker broad peaks[1]. The proton chemical shift dispersion of the broader peaks is slightly greater than that of the intense peaks, but in all cases the dispersion is much less than for the free protein. The decreased number of cross-peaks observed in this spectrum

[1] In addition, seven very weak but relatively sharp signals were observed, at positions distinctly different from those of the free protein. The low intensity of these peaks and their relatively narrow linewidth suggests that they reflect the presence of a small amount of protein degradation products.

provides evidence for highly heterogeneous motional properties of the talin fragment in the complex, and the narrow linewidths and limited chemical shift dispersion of those cross-peaks which are observed suggests that they arise from highly mobile and predominantly unstructured regions of talin 755-889.

The resonances corresponding to the mobile regions of talin 755-889 in the complex were assigned using a standard set of triple-resonance experiments and are labelled in Figure 4b. For the majority of the residues from these regions relatively strong cross-peaks were observed in the HNCACB and HNCACO spectra, confirming the high mobility of the corresponding residues. The resonances with the sharpest lines arise from residues close to the N- and C-termini that are mobile and unstructured in the complex as they are in the free protein. As shown in Figure 4c, the intensity of the cross-peaks decreases with the distance from the termini, and cross-peaks are visible for residues 756-762 at the N-terminus and 879-889 at the C-terminus of the bound talin fragment. The remainder of the visible cross-peaks can be assigned to a continuous stretch of residues 791-820, corresponding, in free talin 755-889, to helix H2 and the loops connecting it to the neighbouring helices. Within this stretch, the most intense cross-peaks correspond to the large loop between helices H1 and H2. The chemical shift index (Wishart and Sykes, 1994) confirms the lack of any secondary structure in the assigned regions. The spectrum thus provides clear evidence that helix H2 of talin 755-889 unfolds to a flexible random coil on formation of a complex with Vh'.

At the same time, the regions of talin 755-889 corresponding to helices H1, H3 and H4 appear to be immobilised in the complex, as none of the residues from these helices have observable cross-peaks in the NMR spectrum. The overall molecular weight of a 1:1 complex of Vh' with talin 755-889 (~45 kDa) is not so great that it would be expected to make the resonances completely unobservable for [^{2}H, ^{15}N]-labelled protein. Conformational exchange processes on the millisecond timescale might lead to additional exchange broadening of the resonances of helix H4, which interacts with Vh'. However, even if this was the case, it does not address the fact that resonances corresponding to helices H1 and H3 are also unobserved. This is particularly striking for the resonances corresponding to helix H1, which is connected to the rest of the molecule in the complex by a long (>30 residue) unstructured region which does give rise to observable resonances. The pattern of observable resonances in the NMR spectra suggest that helices H1 and H3 must be immobilised in the complex through their own interactions with Vh'. The unfolding of helix H2 and the binding of helix H4 to Vh' will leave exposed large hydrophobic patches on the surfaces of helices H1 and H3, and interactions of these with additional Vh' molecules would explain the stoichiometry of >1:1 indicated by the NMR titration and the PAGE experiments. The molecular mass of a complex involving several Vh' molecules might be sufficiently large to explain the failure to observe [^{1}H,^{15}N] HSQC signals from the residues of helices H1, H3 and H4.

Discussion

The NMR data reported here shows that the talin fragment 755-889 forms a stable 4-helix bundle with a topology and structure similar to the 4-helix bundle 656-789 from the larger preceding fragment 482-789, whose crystal structure we have recently determined (Papagrigoriou *et al.,* 2004); combining these two structures leads to a model for the talin region 482-889 consisting of a 5-helix bundle packed against a 7-helix bundle. The sequence of the remaining ~1600 residues of the talin rod has very similar characteristics to talin 482-889, suggesting that it may comprise similar domains comprising 5- and 7-helix bundles, perhaps linked by unstructured regions. The C-terminal end of the model structure is accessible to the solvent and the sequence immediately following contains a number of charged and polar residues (Figure 1d), suggesting formation of an unstructured loop; the model could thus easily accommodate an extension of the structure to build up the full talin rod. A surface hydrophobic patch between helices H1 and H4 of talin 755-889 extends from one end to the middle of the 7-helix bundle, and is similar to the area of contact between the 5- and the 4-helix bundles in talin 482-789. It may be involved in a hydrophobic contact with helical bundle domains formed by adjacent residues of the talin rod; this would create a staggered domain arrangement, similar to that observed in talin 482-789. However, the repetitive nature of the predicted amphipathic helices and the high alanine content make it difficult to be sure whether the proposed structure of the first 400 residues is indeed repeated along the whole talin rod.

The structures of talin rod fragments 482-789 and 755-889 show that the amino-acid residues known to be important for vinculin binding are buried in the core of the helical bundle, implying that these conformations would be inactive in terms of Vh' binding. This is clearly seen in a direct comparison of the location of the vinculin binding residues in the structures of talin 755-889 and of the vinculin Vh'–VBS2 peptide complex (Figure 3). This would also be true of the modelled 7-helix bundle conformation of talin 656-889. Therefore, there must be a significant conformational rearrangement of these helical bundles in order to permit binding to Vh'. We earlier obtained indirect evidence for this by showing that removal of the C-terminal helix of the talin 482-655 5-helix bundle led to partial unfolding of the structure, and to a marked increase in affinity for Vh' (Papagrigoriou *et al.,* 2004). The NMR analysis of the interaction of talin 755-889 with Vh' reported here presents the first direct experimental characterisation of the large structural rearrangement of talin which accompanies (and permits) binding to vinculin. The main feature of the structural change is the complete unfolding of helix H2, whose resonances are seen as characteristic of a highly flexible, unstructured region of the protein. In addition to helix H4, which contains the known vinculin binding site, helices H1 and H3 are also immobilised in the complex. This, together with the results of NMR titration and native PAGE experiments, indicates that more than one molecule of Vh' can bind to this 4-helix fragment. This unexpected observation raises the possibility that *in vivo,* the vinculin head can bind to the talin rod at more than the three sites

identified earlier (Hemmings *et al.*, 1996; Bass *et al.,* 1999). The NMR spectra also clearly indicate that the talin rod becomes more flexible, due to the unfolding of the helical bundles, when vinculin binds.

Figure 5 illustrates that it is stereochemically possible for three vinculin head molecules to bind to helices H1, H3 and H4 of the unfolded talin 755-889. While the regions of the talin rod corresponding to H1 and H3 had not previously been identified as vinculin binding sites, the sequence comparison in Figure 5b shows that the postulated vinculin contact residues in these helices are sufficiently similar to those in VBS1, VBS2 and VBS3 to make vinculin binding by H1 and H3 plausible. Interestingly, F-actin and PIP2 have been reported to induce formation of vinculin dimers (Johnson and Craig, 2000) and trimers (Johnson and Craig, 2000; Huttelmaier *et al.,* 1998) respectively via self association sites in the vinculin tail domain, and talin VBS2 may favour recruitment of such vinculin complexes. The fact that previously unrecognised vinculin binding helices exist within the talin rod, and that vinculin increases the flexibility of the talin rod, suggests that vinculin will have a marked effect on the structure of the initial talin/actin complexes assembled on the cytoplasmic face of integrins. This would be consistent with the finding that although vinculin is not required for the assembly of focal adhesions (Xu *et al.,* 1998), it does stabilise these structures (R.M. Saunders, M.R. Holt, G. A. Dunn and D.R. Critchley, unpublished data); this may explain why vinculin suppresses cell migration.

Methods

Expression of recombinant talin and vinculin polypeptides

Limited proteolysis with trypsin of a chick talin construct spanning residues 727-965 led to a resistant 14kDa fragment which was identified as comprising residues 755-889. The cDNA encoding murine talin residues 755-889 was synthesised by PCR using a mouse talin-1 cDNA as template, cloned into the expression vectors pET-15b and pET-11a (Novagen, Merck Biosciences, Nottingham) and expressed in *E. coli* BL21 (DE3) cultured either in 2YT for unlabelled protein, or in minimal media (Marley *et al.,* 2001) for preparation of labelled samples for NMR. Recombinant His-tagged talin 755-889 was purified by nickel-affinity chromatography following standard procedures. The His-tag was removed by cleavage with thrombin, and the protein further purified by ion-exchange chromatography and gel-filtration. Recombinant untagged talin 755-889 fragment was purified by ion-exchange chromatography followed by gel-filtration. Both proteins were judged to be pure by SDS-PAGE and were authenticated by N-terminal sequencing. Recombinant His-tagged chick vinculin head (Vh', residues 1-258) was expressed in pET-15b and purified as described for the talin polypeptides. Protein concentrations were determined using the BCA Protein Assay (Pierce, Rockford, IL, U.S.A.).

NMR Spectroscopy

NMR experiments for resonance assignment and structure determination of the talin 755-889 fragment were performed in buffer comprising 20mM sodium phosphate, 50mM NaCl, 0.02 % (w/v) NaN_3 at pH 6.5. ^2H_2O was added to a final concentration of 10% (v/v) as an internal lock. The protein was concentrated to 1.5mM using a centrifugal concentrator with a 5kDa cut-off membrane (Vivascience, Germany). No spectral differences were observed between thrombin-cleaved or untagged samples. For experiments in 100% ^2H_2O, unlabelled protein was concentrated to 1mM, flash-frozen in liquid nitrogen, lyophilised and resuspended in the required volume of ^2H_2O. For the titration of talin 755-889 with Vh', the buffer used was 20mM sodium phosphate, 200mM NaCl, 5mM DTT at pH 6.5.

NMR spectra of talin 755-889 were obtained at 30^{o}C using Bruker AVANCE DRX 600 or Varian INOVA 800 (Biomedical NMR Centre, NIMR, Mill Hill) spectrometers. Spectra of the talin 755-889/Vh' complex were obtained at 15^{o}C using a Bruker AVANCE DRX 600 equipped with a CryoProbe. All spectra were processed using nmrPipe (Delaglio *et al.,* 1995) and analysed with NMRView (Johnson and Blevins, 1994). Backbone and side-chain assignments were obtained using standard triple- and double-resonance experiments (Sattler *et al.,* 1999). The program AUTOASSIGN (Moseley *et al.,* 2001) was used for the backbone assignments of talin 755-889. Prochiral CH_3 groups of all Val and Leu residues apart from Leu 56 and Leu 106 were assigned

using [^{1}H,^{13}C] CT-HSQC spectra of 10% ^{13}C labelled samples (Neri et al., 1989).

NMR structure calculation

Distance restraints were obtained from the following experiments: 3D ^{15}N-edited NOESY-HSQC (600 MHz, 100 ms), ^{13}C-edited NOESY-HSQC in H_2O (800 MHz, 100 ms), ^{13}C-edited HMQC-NOESY in D_2O (800 MHz, 100 ms) and 2D NOESY in $^{2}H_2O$ (600 MHz, 100 ms). All NOESY peaks were picked automatically using NMRView and noise and artefact peaks were removed manually. Cross-peak intensities were used to evaluate target distances. Initial models were generated with CYANA using the CANDID (Herrmann *et al.,* 2002) method for NOESY cross-peak assignment and calibration. These models were used as initial structures in structure calculation by ARIA (Linge *et al.,* 2001). The acceptance tolerances in the standard protocol of ARIA1.2 were modified to set violation tolerances to 4.0, 2.0, 1.0, 0.5, 2.0, 1.0, 0.5 Å for iterations 2-8, respectively, with iteration 1 containing the initial models. Floating chirality was restricted to CH_2, NH_2 and the chirally unassigned CH_3 groups of Leu 56 and Leu 106. Cross-peaks rejected by ARIA were checked manually and, if found reliable, added to the calculation. 100 structures were calculated at each iteration, the 20 lowest energy retained and 10 used for the restraint analysis. The 20 lowest energy structures from iteration 8 were further refined in the presence of explicit water molecules. The structural statistics are presented in Table 1; the set of 20 lowest energy structures has been submitted to the Protein Data Bank (1U89). Structures were analysed using VMD (Humphrey et al., 1996). Figures were generated with VMD, PYMOL (http://www.pymol.org) and MolScript (Kraulis, 1991).

Molecular modelling

The model of the combined fragment 482-889 based on the X-ray structure of talin 482-789 (Papagrigoriou *et al.,* 2004) and the NMR structure of talin 755-889 was generated using ARIA 1.2 protocols for NMR structure calculations. A set of interproton distance restraints and backbone dihedral angle restraints were calculated for each experimental structure and combined during the structure calculation. In case of the X-ray structure protons were added with a standard CNS (Brunger *et al.,* 1998) protocol prior to restraint calculation. Interproton distances less than 6Å between all non-exchangeable and backbone NH protons in α-helices were selected as the target distances for the restraints. For methylene and methyl groups a single effective distance calculated according to the SUM option of the CNS distance target function was evaluated and used during the model calculation. The upper and lower tolerances were set to ±30% of the target distance. Backbone dihedral angles for the helical regions of the structures were evaluated using a standard CNS protocol. Models satisfying these restraints were calculated for the regions 486-781, 656-781 and 755-888, corresponding to the experimentally determined structures, and for 656-888 and 486-888, corresponding to the combined 7- and 12-helix fragments. 200 structures were generated for

each fragment and the 20 best were subjected to further refinement in the presence of explicit water molecules. The numbers of restraints and rmsd differences between the modelled and experimental structures are presented in Table 2; the lowest energy theoretical model has been submitted to the Protein Data Bank (1XWX).

X-ray crystallography

Recombinant His-tagged chick Vh' was expressed and purified as described earlier (Papagrigoriou *et al.,* 2004). The purified protein was transferred into 20 mM Tris-HCl, pH 8, 0.2M NaCl, 5mM DTT, concentrated to 8.9 mg/ml, aliquoted and stored at -180°C. A peptide corresponding to chick talin VBS2 (residues 849 to 879, corresponding to helix H4 in talin 755-889) was synthesised and HPLC-purified (Alpha Diagnostics, San Antonio, USA). The peptide was dissolved in water and added to the recombinant Vh' at an equimolar ratio. Crystals of space group $P2_12_12$ were grown from 0.1M Tris-HCl, 10mM $MgCl_2$, 21% PEG 8000, pH 7.5, at 20°C. Data were collected at the ESRF, beamline 14-2, using an ADSC CCD detector (λ=0.933) and the structure was solved by molecular replacement using AmoRe (CCP4 suite) with the structure of the Vh'–VBS3 peptide complex (our unpublished data) as a search model. The Vh'–VBS2 model was built using XtalView (McRee, 1999) and refinement was carried out using REFMAC (CCP4 suite), to a final R factor = 0.242 for all data between 30Å and 2.38Å and R_{free} = 0.322. The main chain torsion angles of 88.9% of the residues lie within most favored regions, 7.5% in additional favoured regions, 2.4% in generously allowed regions. Data collection and refinement statistics are given in Supplementary Table 1. The structure has been submitted to the Protein Data Bank (1U6H).

PAGE analysis of talin 755-889 binding to Vh'

For both the talin 482-636 and 755-889 titrations, a 0.15mM vinculin head (Vh') solution was added to 14μM talin. The talin/vinculin molar ratios tested were 1:4, 1:2, 1:1, 1:2, 1:3 and 1:4. The final volume of each assay was 20μl in a buffer of 20mM sodium phosphate, 200mM NaCl, 5mM DTT, pH 6.5. 20μl of 2x Tris-Glycine sample buffer was added to each sample prior to electrophoresis for 2 hr at 125V using 12% Novex® Tris-Glycine gels. Gels were stained using SimplyBlue™ Safe stain (buffer, gels and stain from Invitrogen Corporation, UK).

Acknowledgements

This work was supported by the Biotechnology and Biological Sciences Research Council and the Wellcome Trust. We are grateful for access to the 800MHz NMR spectrometer of the Biomedical NMR Centre at the National Institute for Medical Research, Mill Hill, London, to Dr. G. Kelly for running the 800MHz spectra, and to Drs. M. Carr, M. Pfuhl and F. Muskett for advice and assistance.

FIGURE CAPTIONS

Figure 1
Solution structure of talin 755-889

a. Stereo view of the superposition (using backbone atoms in the helices) of the 20 lowest energy structures consistent with the NMR data. Only the structural core region, residues 763-878, is shown, not the disordered N- and C-termini. **b.** Stereo view of a representative low energy structure showing the residues comprising the hydrophobic clusters and the 'threonine belt' – see text. **c.** Representations of the NMR structure of talin 755-889 (left) and the X-ray structure of talin 656-789 (right). The order of the helices from the N- to the C-terminus is represented by the colour, in the order red, green, blue, purple. Talin 755-889 has the same orientation in **a-c**. **d.** The sequence of talin 755-889 indicating the positions of the α-helices, corresponding to the colours in **c**.

Figure 2

Model of the N-terminal region of the talin rod on the basis of the experimental structures of the isolated fragments.

a. Superposition of the X-ray structure of talin 656-789 (orange) and the NMR structure of talin 755-889 (green) using the common helix 763-780. There is a partial overlap of one helix between the two fragments. **b.** Model for the region 656-889 (cyan) that retains contacts experimentally observed for the isolated fragments 656-789 and 755-889, but avoids the clash between the helices. The structures of the isolated domains 656-789 (blue) and 755-889 (red) are superimposed on the corresponding regions of the model. **c.** Side view of the model shown in **b**, in ribbon representation. **d.** Model of the N-terminal region of the talin rod, residues 482-889; residues 482-659 are shown in blue, 660-756 in red, 757-786 in orange and 787-889 in purple.

Figure 3

Structure of vinculin Vh' complexed with the talin VBS2 peptide.

a. Stereo view of the final F_o-F_c electron density map, contoured at 3.0σ, of the talin peptide (green) bound to helices α1 and α2 of the N-terminal bundle of the vinculin head domain Vh' (yellow) as seen in the Vh':VBS2 crystal structure. **b.** Location of the vinculin binding residues of VBS2 in the complex with Vh' and in free talin 755-889. The structure of talin 755-889 (*left*) and the structure of the Vh' – VBS2 peptide complex (*right*) shown with the VBS2 (H4) region in the same orientation in each case. The VBS2 helix is shown as a ribbon, other helices as semi-transparent cylinders. Side-chains of the VBS2 residues involved in the interaction with Vh' are shown in red in both structures, illustrating the fact that these residues are buried in the hydrophobic core of both structures.

Figure 4

Interaction between Vh' and talin 755-889.

a,b. [^{1}H,^{15}N]-HSQC spectra of uniformly ^{15}N-labelled talin 755-889; **a**, free in solution and **b**, in the presence of a 3-fold molar excess of Vh'. The assignments of the resolved cross-peaks observed in the complex state are shown in **b**. Low intensity peaks observed in the complex and referred to in the text are indicated by *. Two cross-peaks were observed for Thr 758 and Glu 759 due to partial loss of the N-terminal Met 755, confirmed by protein sequencing. **c.** Intensities (arbitrary units) of the cross-peaks in the [^{1}H,^{15}N]-HSQC spectrum of ^{15}N-labelled talin 755-889 in the presence of a 3-fold molar excess of Vh' as a function of sequence position; the positions of the helices in free talin 755-889 are indicated by the black bars. **d.** Native PAGE gels illustrating the formation of the complexes of Vh' with talin 755-889 (top) and talin 482-636 (bottom). Lane 1: talin fragment alone lane 2: Vh' alone. Each talin fragment was at a fixed concentration of 14μM, and Vh' was added to give [talin]:[Vh'] molar ratios of 4:1, 2:1, 1:1, 1:2, 1:3, 1:4 in lanes 3-8 respectively.

Figure 5

Schematic diagram of the interaction between the vinculin head (Vh') and talin 755-889.

a. The binding of Vh' to the VBS2 site (H4) requires the opening of the 4-helix bundle and unfolding of helix H2. This exposes hydrophobic surfaces of helices H1 and H3 which are thus available for interactions with Vh', leading to a complex involving more than one Vh' molecule. The Vh'–VBS2 (H4) complex has a well-defined conformation, a 5-helix bundle, while the interactions with H1 and H3 may have lower affinity and specificity. Talin 755-889 is shown in green, Vh' in red and light brown. In the model of the complex, the Vh' shown in red corresponds to the experimentally determined position in the Vh'–VBS2 peptide structure, while the Vh' molecules in light brown have been positioned on the assumption that the interaction of Vh' with H1 and H3 is similar to that with H4. The free Vh' is represented by the Vh' structure from the Vh'/Vt complex (PDB 1rke). **b.** Alignment of the vinculin binding sequences of talin, VBS1-3, and helices H1 and H3 of talin 755-889. Residues corresponding to those involved in the intermolecular interaction in the Vh'–VBS2 complex are highlighted in red in each sequence.

References

Albiges-Rizo, C., Frachet, P., and Block, M.R. (1995). Down regulation of talin alters cell adhesion and the processing of the α5β1 integrin. J. Cell Sci. 108, 3317-3329

Bakolitsa, C., dePereda, J.M., Bagshaw, C.R., Critchley, D.R., and Liddington, R.C. (1999). Crystal structure of the vinculin tail suggests a pathway for activation. Cell *99,* 603-613

Barsukov, I.L., Prescot A., Bate N., Patel B., Floyd D.N., Bhanji N., Bagshaw C.R., Letinic K., Di Paolo G., De Camilli P., Roberts G.C.K., and Critchley D.R. (2003).Phosphatidylinositol phosphate kinase type 1γ and β1-integrin cytoplasmic domain bind to the same region in the talin FERM domain. J. Biol. Chem. *278,* 31202-31209

Bass, M.D., Smith, B.J., Prigent, S.A., and Critchley, D.R. (1999). Talin contains three similar vinculin-binding sites predicted to form an amphipathic helix. Biochem. J. *341,* 257-263

Bolton, S. J., Barry S.T., Mosley H., Patel B., Jockusch B.M., Wilkinson J.M., and Critchley D.R. (1997). Monoclonal antibodies recognizing the N- and C- terminal regions of talin disrupt actin stress fibers when microinjected into human fibroblasts. Cell Motil. Cytoskeleton *36,* 363-376

Brown, N.H., Gregory S.L., Rickoll W.L., Fessler L.I., Prout M., White R.A.H., and Fristrom J.W. (2002). Talin is essential for integrin function in Drosophila. Dev. Cell *3,* 569-579

Brunger A.T., Adams P.D., Clore G.M., DeLano W.L., Gros P., Grosse-Kunstleve R.W., Jiang J.S., Kuszewski J., Nilges M., Pannu N.S., Read R.J., Rice L.M., Simonson T., and Warren G.L. (1998). Crystallography and NMR system (CNS): a new software system for macromolecular structure determination. Acta Cryst. *D54*, 905-921

Calderwood, D.A. (2004). Integrin activation. J Cell Sci. *117,* 657-666

Chen, H.C., Appeddu P.A., Parsons, J.T., Hildebrand, J.D., Schaller, M.D., and Guang, J.L. (1995). Interaction of focal adhesion kinase with the cytoskeletal protein talin. J. Biol. Chem. *270*, 16995-16999

Cornilescu, G., Delaglio, F., and Bax. A. (1999). Protein backbone angle restraints from searching a database for chemical shift and sequence homology. J.Biol. NMR *13*, 289-302

Cram, E.J., Clark, S.G., and Schwarzbauer, J.E. (2003). Talin loss-of-function uncovers roles in cell contractility and migration in C. elegans. J. Cell Sci. *116,* 3871-3878

Delaglio, F., Grzesiek, S., Vuister, G.W., Zhu, G., Pfeifer, J., and Bax, A. (1995). Nmrpipe - a

multidimensional spectral processing system based on Unix pipes. J. Biomol. NMR *6*, 277-293

Di Paolo, G., Pellegrini L., Letinic K., Cestra G., Zoncu R., Voronov S., Chang S.H., Guo J., Wenk M.R., and De Camilli P. (2002). Recruitment and regulation of phosphatidylinositol phosphate kinase type Iγ by the FERM domain of talin. Nature *420,* 85-89

Garcia-Alvarez, B., de Pereda J.M., Calderwood D.A., Ulmer T.S., Critchley D., Campbell I.D., Ginsberg M.H., and Liddington R.C. (2003) Structural determinants of integrin recognition by talin. Mol. Cell *11,* 49-58

Giannone, G., Jiang, G., Sutton, D.H., Critchley, D.R., and Sheetz, M.P. (2003). Talin1 is critical for force-dependent reinforcement of initial integrin-cytoskeleton bonds but not tyrosine kinase activation. J Cell Biol. *163,* 409-419.

Gilmore, A. P., and Burridge, K. (1996). Regulation of vinculin binding to talin and actin by phosphatidylinositol-4-5-bisphosphate. Nature *381,* 531-535

Hemmings, L., Rees D.J.G., Ohanian V., Bolton S.J., Gilmore A.P., Patel B., Priddle H., Trevithick J.E., Hynes R.O., and Critchley D.R. (1996). Talin contains three actin-binding sites each of which is adjacent to a vinculin-binding site. J. Cell Sci. *109,* 2715-2726

Herrmann, T., Guntert, P., and Wüthrich, K. (2002). Protein NMR structure determination with automated NOE assignment using the new software CANDID and the torsion angle dynamics algorithm DYANA. J. Mol. Biol. *319*, 209-227

Holm, L., and Sander, C. (1997). DALI/FSSP classification of three dimensional protein folds. Nucleic Acids Res. *25*, 231–234

Humphrey, W., Dalke, A. and Schulten, K. (1996). VMD - Visual Molecular Dynamics. J. Molec. Graphics *14*, 33-38

Huttelmaier, S., Mayboroda, O., Harbeck, B., Jarchau, T., Jockusch, B.M., and Rudiger, M. (1998). The interaction of the cell-contact proteins VASP and vinculin is regulated by phosphatidyl-inositol-4,5-bisphosphate. Curr. Biol. *8*, 479-488

Izard, T., Evans G., Borgon R.A., Rush C.L., Bricogne G., and Bois P.R.J. (2004) Vinculin activation by talin through helical bundle conversion. Nature *427,* 171-175

Izard, T., and Vonrhein, C. (2004). Structural basis for amplifying vinculin activation by talin. J. Biol. Chem.. *279*, 27667-27678

Jiang, G., Giannone, G., Critchley, D.R., Fukumoto, E., and Sheetz, M.P. (2003). Two-piconewton slip bond between fibronectin and the cytoskeleton depends on talin. Nature *424,* 334-337

Jockusch, B. M., and Rudiger, M. (1996). Crosstalk between cell adhesion molecules: vinculin as a paradigm for regulation by conformation. Trends Cell Biol. *6,* 311-315

Johnson, B.A., and Blevins, R.A. (1994). NMR VIEW - a computer-program for the visualization and analysis of nmr data. J. Biomol. NMR *4*, 603-614

Johnson, R.P., and Craig, S.W. (2000) Actin activates a cryptic dimerization potential of the vinculin tail domain. J. Biol. Chem. *275*, 95-105

Kim, M., Carman, C.V., and Springer, T.A. (2003). Bidirectional transmembrane signaling by cytoplasmic domain separation in integrins. Science *301,* 1720-1725

Kraulis, P.J. (1991). MOLSCRIPT: A program to produce both detailed and schematic plots of protein structures. J. Appl. Crystallog. *24*, 946-950

Laskowski, R.A., Rullmann, J.A.C., MacArthur, M.W., Kaptein, R., and Thornton, J.M. (1996). AQUA and PROCHECK-NMR: programs for checking the quality of protein structures solved by NMR. J. Biomol. NMR *8*, 477-486

Ling, K., Doughman, R.L., Firestone, A.J., Bunce, M.W., and Anderson R.A. (2002). Type Iγ phosphatidylinositol phosphate kinase targets and regulates focal adhesions. Nature *420,* 89-93

Linge, J.P., O'Donoghue, S., and Nilges, M. (2001). Assigning ambiguous NOEs with ARIA. Meth. Enzymol. *339*, 71-90.

Liu, S., Calderwood, D.A., and Ginsburg, M.H. (2000). Integrin cytoplasmic domain-binding proteins. J. Cell Sci. *113,* 3563-3571.

Marley, J., Lu, M., and Bracken, C. (2001). A method for efficient isotopic labeling of recombinant proteins. J. Biomol NMR. *20*, 71-75

Martel, V., Racaud-Sultan C., Dupe S., Marie C., Paulhe F., Galmiche A., Block M.R., Albiges-Rizo C. (2001). Conformation, localization, and integrin binding of talin depend on its interaction with phosphoinositides. J. Biol. Chem. *276,* 21217-21227

McCann, R. O., and S.W. Craig. (1997). The I/LWEQ module: a conserved sequence that signifies F-actin binding in functionally diverse proteins from yeast to mammals. Proc. Natl. Acad. Sci. USA *94*, 5679-5684

McRee DE. (1999). XtalView Xfit - A versatile program for manipulating atomic coordinates and electron density. J. Struct. Biol. *125*, 156-165

Monkley, S. J., Zhou X.H., Kinston S.J., Giblett S.M., Hemmings L., Priddle H., Brown J.E., Pritchard C.A., Critchley D.R., and Fassler R. (2000). Disruption of the talin gene arrests mouse development at the gastrulation stage. Devel. Dynamics *219,* 560-574

Moseley, H.N.B., Monléon, D., and Montelione, G.T. (2001). Automatic determination of protein backbone resonance assignments from triple resonance NMR data. Meth. Enzymol. *339*, 91-108

Neri, D., Szyperski, T., Otting, G., Senn, H. and Wüthrich, K. (1989). Stereospecific nuclear magnetic resonance assignments of the methyl groups of valine and leucine in the DNA-binding domain of the 434 repressor by biosynthetically directed fractional carbon-13 labeling. Biochemistry *28*, 7510-7516

Nuckolls, G.H., Romer, L.H., and Burridge, K. (1992). Microinjection of antibodies against talin inhibits the spreading and migration of fibroblasts. J. Cell Sci. *102,* 753-762

Papagrigoriou, E., Gingras, A.R., Barsukov, I.L., Bate, N., Fillingham, I.J., Patel, B., Frank, R., Ziegler, W.H., Roberts, G.C.K., Critchley, D.R., and Emsley, J. (2004). Activation of a vinculin binding site in the talin rod involves rearrangement of a five helix bundle. EMBO J. *23*, 2942-2951

Priddle, H., Hemmings L., Monkley S., Woods A., Patel B., Sutton D., Dunn G.A., Zicha D., and Critchley D.R. (1998). Disruption of the talin gene compromises focal adhesion assembly in undifferentiated but not differentiated ES cells. J. Cell Biol. *142,* 1121-1133

Sattler, M., Schleucher, J. and Griesinger, C. (1999). Heteronuclear multidimensional NMR experiments for the structure determination of proteins in solution employing pulsed field gradients. Prog. NMR Spectrosc. *34*, 93-158

Tadokoro, S., Shattil S.J., Eto K., Tai V., Liddington R.C., de Pereda J.M., Ginsberg M.H., and Calderwood D.A. (2003). Talin binding to integrin beta tails: a final common step in integrin activation. Science *302,* 103-106

Tremuth, L., Kreis S., Melchior C., Hoebeke J., Ronde P., Plancon S., Takeda K., and Kieffer N. (2004). A fluorescence cell biology approach to map the second integrin binding site of talin to a 130-amino acid sequence within the rodd domain. J. Biol. Chem., *279*, 22258-22266

Winkler, J.H., Lunsdorf, H., and Jockusch, B.M. (1997). Energy-filtered electron microscopy

reveals that talin is a highly flexible protein composed of a series of globular domains. *Eur. J.* Biochem. *243,* 430-436

Wishart, D.S., and Sykes, B.D. (1994). The ^{13}C chemical-shift index: a simple method for the identification of protein secondary structure using ^{13}C chemical-shift data. J. Biomol. NMR, *4*, 171-180

Xing, B., Jedsadayanmata, A., and Lam, S.C. (2001). Localization of an integrin binding site to the C terminus of talin. J. Biol. Chem. *276,* 44373-44378.

Xu, W., Baribault, H., and Adamson, E.D. (1998). Vinculin knockout results in heart and brain defects during embryonic development. Development *125,* 327-337

Figure1

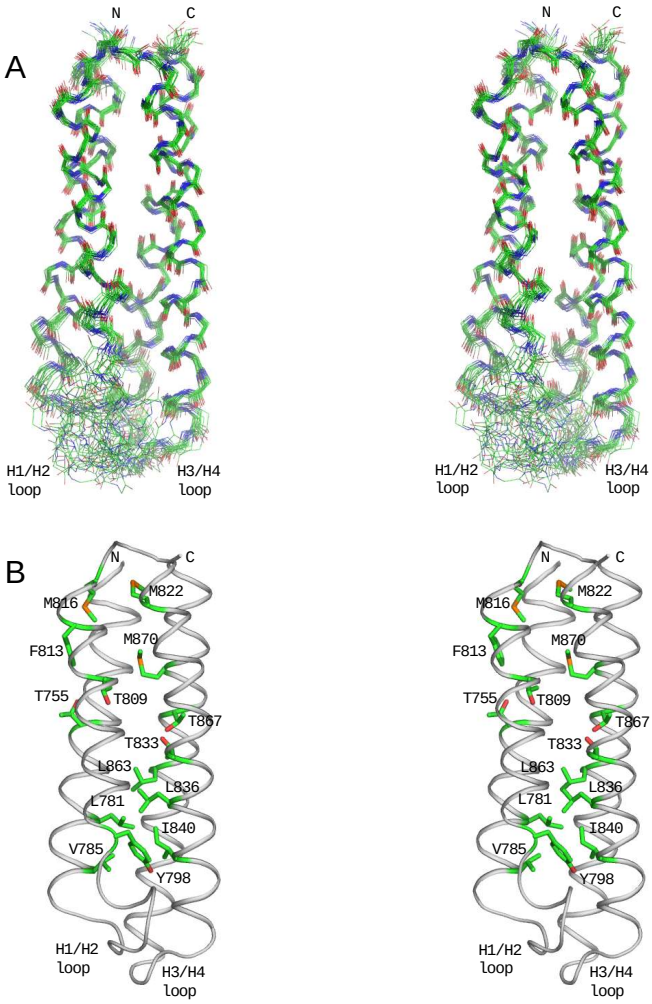

D

```
755                                H1
QAATEDGQLLRGVGAAATAVTQALNELLQHVKAH
789                                H2
ATGAGPAGRYDQATDTILTVTENIFSSMGDAGEM
823                  H3
VRQARILAQATSDLVNAIKADAEGESDLENSRKL
857                  H4
LSAAKILADATAKMVEAAKGAAAHPDSEEQQQR
```

Figure2

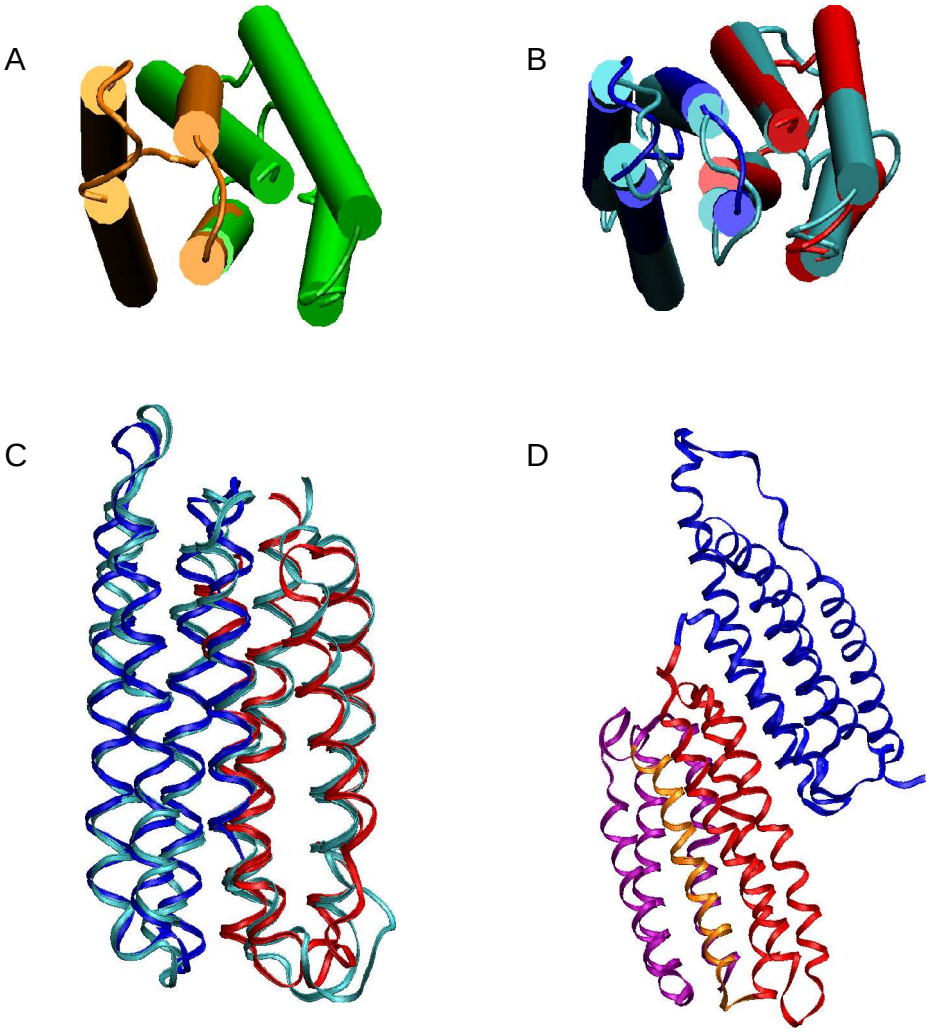

Figure3

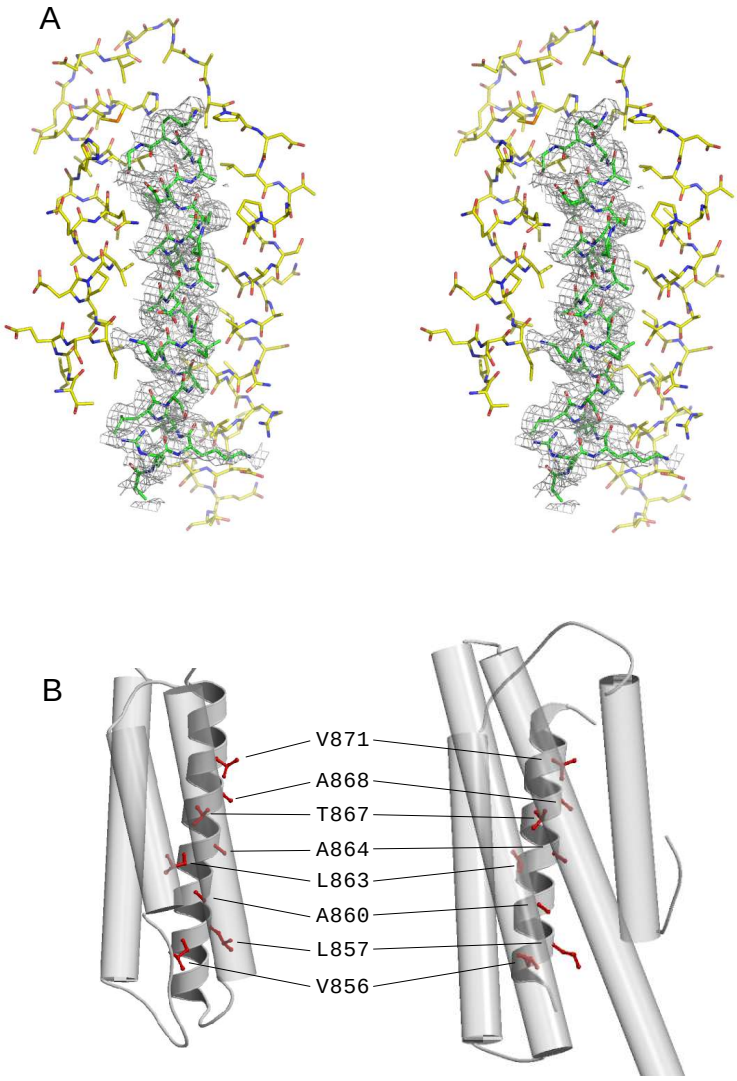

Figure4

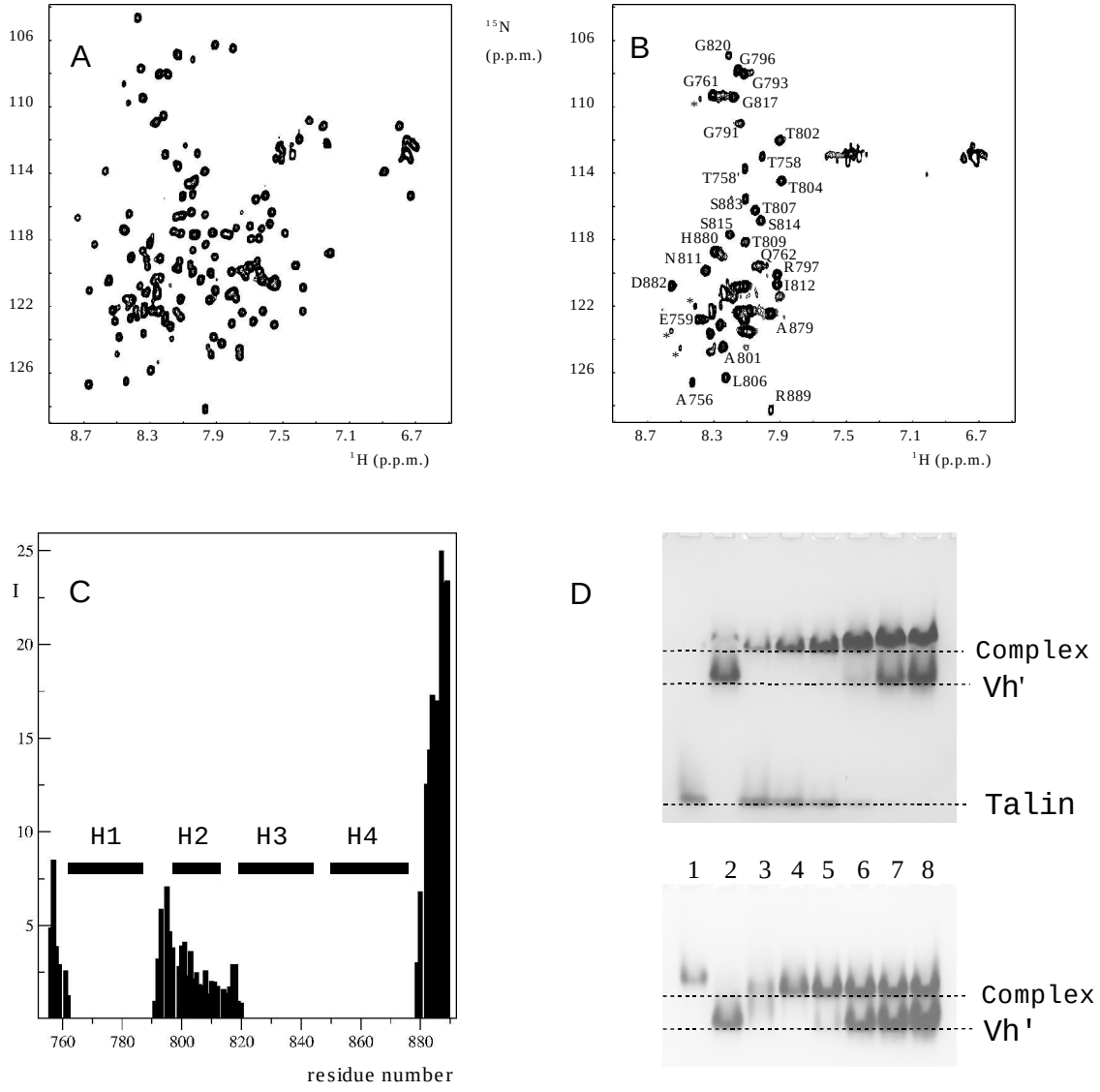
A
B
C
D
^{15}N (p.p.m.)
^{1}H (p.p.m.)
106
110
114
118
122
126
8.7
8.3
7.9
7.5
7.1
6.7
G820
G796
G761
G793
G817
G791
T802
T758
T758'
T804
S883
T807
S815
S814
H880
T809
N811
Q762
R797
D882
I812
E759
A879
A801
L806
A756
R889
I
25
20
15
10
5
H1
H2
H3
H4
760
780
800
820
840
860
880
residue number
Complex
Vh'
Talin
1 2 3 4 5 6 7 8
Complex
Vh'

Figure5

A

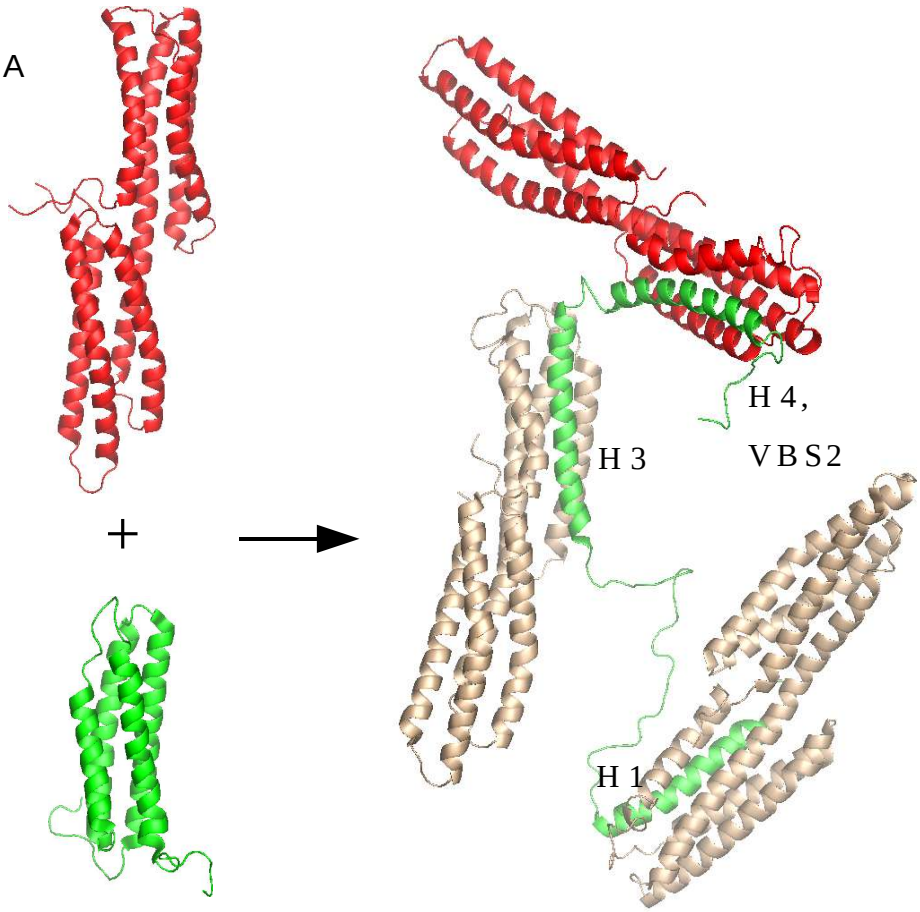

B

VBS1	NGRPLLQAAKGLAGAVSELLRSAQP
VBS2	NSRKLLSAAKILADATAKMVEAAKG
VBS3	TKKELIECARRVSEKVSHVLAALQA
H1	EDGQLLRGVGAAATAVTQALNELLQ
H3	ADGEMVRQARILAQATSDLVNAIKA

Table 1

Solution structure determination of talin 755-889. Experimental restraints and structural statistics

Experimental restraints	
Restraints	
Unique/Ambiguous NOEs	2543/475
Intraresidue	1141/163
Sequential	493/73
Short range (1<|i-j|<5)	361/82
Long range (|i-j|>4)	548/155
φ/ψ dihedral angles[1]	176
Energies (kcal mol^{-1})[2]	
Total	-5608.9±51.3
van der Waals	-1117.9±15.3

Experimental restraints	
NOE	26.0±4.18
R.m.s. deviations[2]	
NOEs (Å) (no violations >0.5 Å)	0.014 ±0.001 / 0.003 ±0.0002
Dihedral restraints (^{o}) (no violations >5^{o})	0.25 ±0.01
Bonds (Å)	0.003 ±0.0001
Angles (^{o})	0.39 ±0.01
Impropers (^{o})	1.07 ±0.1
Ramachandran map analysis (residues 763-878)[3]	
Allowed regions	91.7%
Additional allowed regions	7.1%
Generously allowed regions	0.5%

Experimental restraints	
Disallowed regions	0.7%
Pairwise r.m.s. difference (Å)[4]	
Residues 763-878	1.0 (1.28)
Residues in α-helices	0.43 (0.85)

[1] From chemical shifts using TALOS (Cornilescu *et al.*, 1999)

[2] Calculated in ARIA 1.2 for the 20 lowest energy structures refined in water

[3] Obtained using PROCHECK-NMR (Laskowski *et al.*, 1996)

[4] For backbone atoms; value for all heavy atoms in brackets

Table 2

Modelling the talin fragment 482-889: results of restraint minimisation for different fragments

Fragment	*Distance restraints*	*Dihedral restraints*	*r.m.s.d. (Å)*[1]
656-781	7637	190	0.24
486-781	19865	444	0.35
755-889	7637	192	0.28
656-889	15274	348	0.56 / 0.82

[1]r.m.s.d. calculated for helical regions. For talin 656-889, the first value is for superposition with the experimental structure of talin 656-781, and the second for superposition with talin 755-889.

Supplementary Table 1
X-ray crystal structure of the Vh' – VBS2 peptide complex. Data collection and refinement statistics.

Data Collection

Space group $P2_12_12$. Cell dimensions *a*=52.12Å, *b*=69.15Å, *c*=96.16Å, α=90°, β=90°, γ=90°.

Data range	30-2.38 Å
Completeness	99.68 (99.2)%
Unique reflections	14457
I/σ(I)	10.97 (1.73)
R_{cryst}	0.116 (0.503)

Refinement Statistics

resolution	30-2.38 Å	rmsd bonds	0.020 Å
reflections	14457 (979)	rmsd angles	2.1°
R free	0.322 (0.437)	mean B value	48.8 **Å²**
R factor	0.242 (0.353)		

R_{sym} = Σ|I–<I>|ΣI, I is the observed intensity and <I> is the average intensity of the multiple observations of symmetry-related reflections. R = Σ||Fo| - |Fc̃||Σ|Fo|; R free is calculated for a randomly-selected 5% of the reflections; R factor is calculated for the remaining 95% of the reflections used in refinement. Values in brackets represent the outer resolution shell of 2.44-2.38Å.